Occurrence of tornado outbreaks in the context of solar wind coupling to magnetosphere-ionosphere-atmosphere

Paul Prikryl[1] and Vojto Rušin[2]

[1]Physics Department, University of New Brunswick, Fredericton, NB, Canada; [2]Astronomical Institute, Slovak Academy of Sciences, Tatranská Lomnica, Slovakia

Abstract. A link between the solar wind and occurrence of large tornado outbreaks in the United States is found. Superposed epoch analysis of daily occurrence of tornadoes reveals a peak in the cumulative number of tornadoes near the interplanetary magnetic field (IMF) sector boundary (HCS; heliospheric current sheet) crossings. Most of the large tornado outbreaks are associated with high-density plasma adjacent to HCS and co-rotating interaction regions (CIRs) at the leading edge of high-speed streams (HSSs). Other large tornado outbreaks followed impacts of interplanetary coronal mass ejections (ICMEs) or occurred in the declining phase of major HSSs. We consider the role of the solar wind coupling to the magnetosphere-ionosphere-atmosphere system in severe weather development, mediated by aurorally generated atmospheric gravity waves. While these gravity waves reach the troposphere with attenuated amplitudes, they can contribute to conditional symmetric instability (CSI) release in frontal zones of extratropical cyclones leading to synoptic-scale conditions favoring significant tornado occurrence.

Introduction Tornado outbreaks, particularly in the United States, have a significant impact on human lives and property (Brooks & Doswell, 2001; Tippett, 2014). The occurrence of tornadoes and the associated severe weather, including severe wind and hailstorms, have long been related to the synoptic situation (Fawbush et al., 1951). The latter authors have already discussed an empirical method of forecasting based on several necessary conditions that are known to characterize the synoptic situation during tornado developments, including the presence of conditional instability of the air column and an appreciable lifting of the moist layer near the surface surmounted by a layer of dry air. Many advances have been made in the understanding of the structure and dynamics of tornadoes, and the forecasting of severe weather has progressed (e.g., Bolton et al., 2003; Doswell et al., 1996; 2013; Gallo et al., 2016; Miller et al., 2020). Severe convective storms with an increased occurrence of tornadoes are known to develop in a strong vertical wind shear environment (Púčik et al., 2015, 2021; and references therein).

If changes in environmental factors lead to more unstable conditions in the troposphere, it is of interest to consider possible external influences leading to more intense storms and tornado outbreaks. Prikryl et al. (2009b) have suggested that aurorally generated atmospheric gravity waves (AGWs) can contribute to the release of instabilities, which leads to latent heat release and storminess. Solar wind coupling to the Earth's magnetosphere-ionosphere-atmosphere (MIA) generates globally propagating AGWs from sources in the lower thermosphere at high latitudes. A tendency of significant weather events to occur following the arrivals of corotating interaction regions (CIRs) at the leading edge of solar wind high-speed streams (HSSs) from coronal holes and impacts of interplanetary coronal mass ejections (ICMEs), has been documented (Prikryl et al., 2009a; 2016; 2018; 2019; 2021a, b; Prikryl & Rušin 2023; Prikryl 2024). In this poster, and the supporting material, we investigate the occurrence of tornadoes in the context of solar wind-MIA coupling.

Motivation: "Wilcox effect"

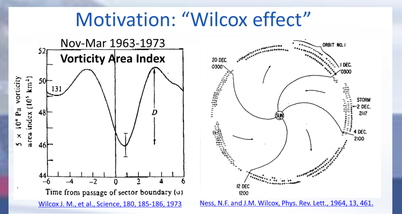

In 1970's a solar physicist John Wilcox discovered a relation between the sector boundaries in the IMF and upper-level vorticity in the troposphere. In mid latitudes in winter, when the extra-tropical cyclones are most active, they found a statistically significant dip in VAI just after the IMF sector boundary crossings (SBCs). They used the superposed epoch (SPE) analysis method.

SPE analysis keyed to the IMF sector boundary (heliospheric current sheet) crossings

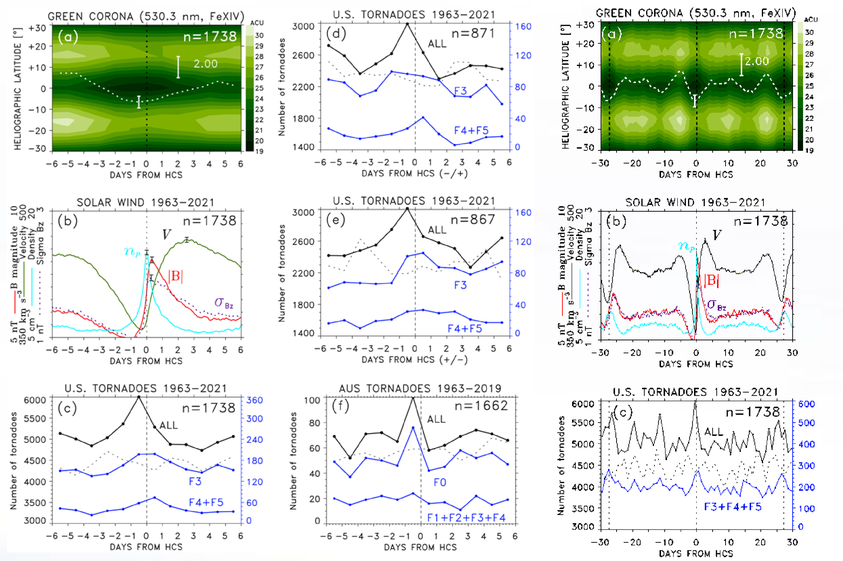

Figure 1. SPE analysis of time series of **(a)** green corona intensity and **(b)** solar wind plasma variables keyed to **(c)** HCS crossings. The cumulative number of tornadoes in the U. S. keyed to (c) all HCS crossings, **(d)** 'toward/away' HCSs, and **(e)** 'away/toward' HCSs. **(f)** The cumulative number of tornadoes in Australia relative to HCS crossings from 1963 to 2019. Dotted lines in panels (c-f) show SPE results for random key times.

Figure 2. SPE analysis of time series of **(a)** green corona intensity, **(b)** solar wind plasma variables and **(c)** the cumulative number of all, as well as the strongest, tornadoes in the U. S., keyed to HCSs ±30 days. The vertical dotted lines are shown for the key time ±27.28 days (the synodic or Carrington rotation). In panel (c), SPE analysis results for random key times are shown in a dotted line.

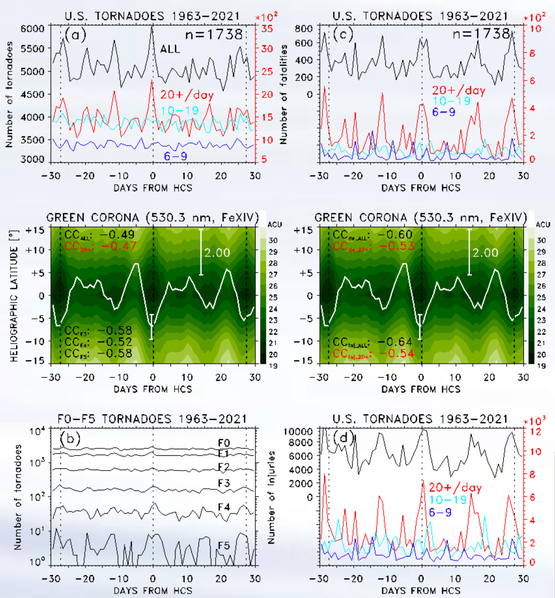

Figure 3. SPE analysis of numbers of tornadoes, fatalities and injuries caused by tornadoes in the U. S. keyed to HCS crossing ±30 days. The vertical dotted lines are shown for the key time ±27.28 days. **(a)** Cumulative numbers of all tornadoes (black line) and tornadoes in tornado outbreaks (color lines). **(b)** Cumulative numbers of tornadoes in logarithmic scale grouped by tornado magnitudes. **(c, d)** Cumulative numbers of tornado fatalities and injuries. The middle panels of the mean green corona intensity are repeated from Fig. 2b. The cross-correlation coefficients between the cumulative numbers of tornadoes/fatalities/injuries and the mean IGC at heliographic latitude 0° are printed.

Occurrence of tornado outbreaks relative to solar wind disturbances

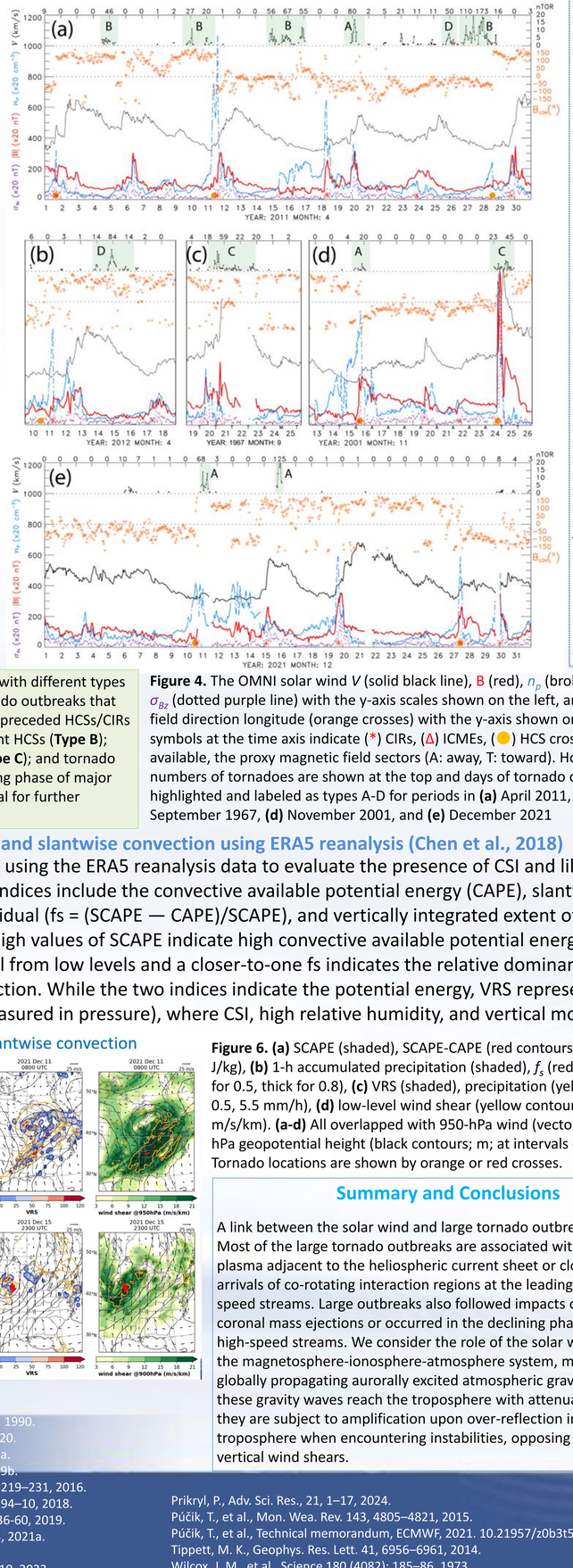

Tornado outbreaks are associated with different types of solar wind disturbances: large tornado outbreaks that closely followed CIRs (**Type A**); closely preceded HCSs/CIRs associated with HDP, including transient HCSs (**Type B**); closely followed impacts of ICMEs (**Type C**); and tornado outbreaks that occurred in the declining phase of major HSSs (**Type D**) (see, Supporting material for further details).

Figure 4. The OMNI solar wind *V* (solid black line), B (red), n_p (broken light blue line), σ_{Bz} (dotted purple line) with the y-axis scales shown on the left, and the magnetic field direction longitude (orange crosses) with the y-axis shown on the right. The symbols at the time axis indicate (*) CIRs, (Δ) ICMEs, (🟡) HCS crossings, and where available, the proxy magnetic field sectors (A: away, T: toward). Hourly and daily numbers of tornadoes are shown at the top and days of tornado outbreaks are highlighted and labeled as types A-D for periods in **(a)** April 2011, **(b)** April 2012, (c) September 1967, **(d)** November 2001, and **(e)** December 2021

Assessment of CSI and slantwise convection using ERA5 reanalysis (Chen et al., 2018)

Several indices are calculated using the ERA5 reanalysis data to evaluate the presence of CSI and likelihood of slantwise convection. These indices include the convective available potential energy (CAPE), slantwise CAPE (SCAPE), fractional SCAPE residual (fs = (SCAPE — CAPE)/SCAPE), and vertically integrated extent of realizable symmetric instability (VRS). High values of SCAPE indicate high convective available potential energy for a slantwise ascending air parcel from low levels and a closer-to-one fs indicates the relative dominance of slantwise over upright convection. While the two indices indicate the potential energy, VRS represents the thickness of the air layer (measured in pressure), where CSI, high relative humidity, and vertical motion coexist.

Assessment of CSI and slantwise convection

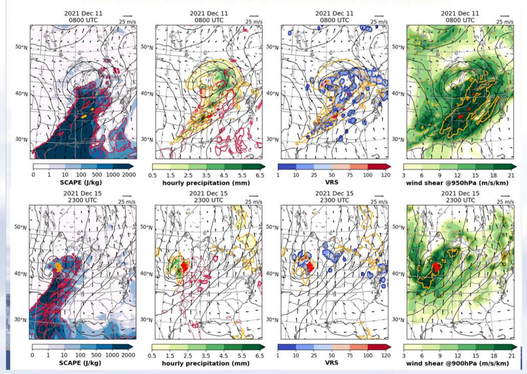

Figure 6. (a) SCAPE (shaded), SCAPE-CAPE (red contours; 100, 300, 500 J/kg), **(b)** 1-h accumulated precipitation (shaded), f_s (red contours; thin for 0.5, thick for 0.8), **(c)** VRS (shaded), precipitation (yellow contours; 0.5, 5.5 mm/h), **(d)** low-level wind shear (yellow contour; 12, 21 m/s/km). **(a-d)** All overlapped with 950-hPa wind (vectors; m/s), 950-hPa geopotential height (black contours; m; at intervals of 50 m). Tornado locations are shown by orange or red crosses.

Summary and Conclusions

A link between the solar wind and large tornado outbreaks is found. Most of the large tornado outbreaks are associated with high-density plasma adjacent to the heliospheric current sheet or closely follow the arrivals of co-rotating interaction regions at the leading edge of high-speed streams. Large outbreaks also followed impacts of interplanetary coronal mass ejections or occurred in the declining phase of major high-speed streams. We consider the role of the solar wind coupling to the magnetosphere-ionosphere-atmosphere system, mediated by globally propagating aurorally excited atmospheric gravity waves. While these gravity waves reach the troposphere with attenuated amplitudes, they are subject to amplification upon over-reflection in the troposphere when encountering instabilities, opposing winds, and vertical wind shears.

Solar wind – MIA coupling

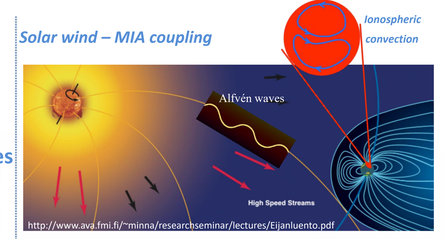

Solar wind coupling to the magnetosphere-ionosphere-atmosphere (MIA) system generates **atmospheric gravity waves** (AGWs) that impact troposphere and may provide a lift of unstable air to release instabilities in the troposphere and to initiate/trigger convection to form cloud and precipitation bands.

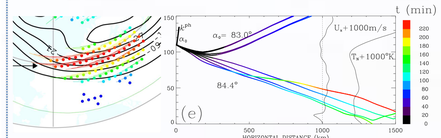

Gravity waves initiate convection

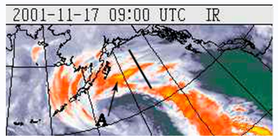

The symmetric instability is an interplay of buoyancy and Coriolis restoring forces:

The slopes of isolines of potential temperature θ and geostrophic momentum Mg in the x-z plane are such that ∂θ/∂z > 0 and ∂Mg/∂x > 0, meaning that atmosphere is stable to purely vertical and horizontal displacements but **unstable to slantwise displacements**.

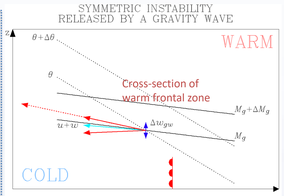

Solar wind Alfvén waves or pressure pulses modulate ionospheric convection, which is a source of gravity waves.

Ray tracing of gravity wave energy using dispersion relation by Hines (1960)

$(\omega^2 - \omega_a^2)\,\omega^2 / C^2 - \omega^2\,(k_x^2 + k_z^2) + \omega_b^2 k_x^2 = 0$

$\omega_a = \gamma g / 2C$ is the acoustic cutoff frequency, γ, C, g are the ratio of specific heats, speed of sound, and acceleration due to gravity,
k_x and k_z are the components of the wave vector **k**.
Brunt-Väisälä (buoyancy) frequency ω_b is defined as
$\omega_b^2 = (\gamma\text{-}1)g^2 / C^2 + (g / C^2)\,(dC^2 / dz)$

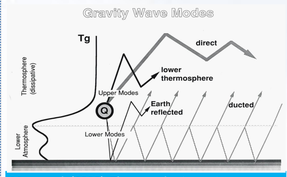

Mayr et al. (1990), Thermospheric gravity waves: Observations and interpretation using the transfer function model. Space Sci. Rev., 54, 297–375.

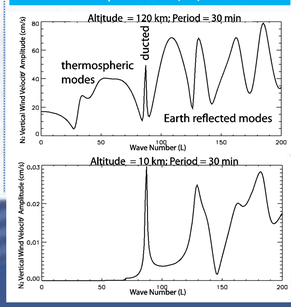

References

Bolton, N., et al., Atmospheric Research, 67–68, 53–72, 2003.
Brooks, H. E. and Doswell, C. A., Weather and Forecasting, 16(1), 168-176, 2001.
Chen T.-C., et al., J. Atmos. Sci. 75, 2425–2443, 2-18.
Doswell, C. A., et al., Weather Forecasting, 11, 560–581, 1996.
Doswell, C. A., et al., AGU Geophysical Monograph 79, 557-571, 2013.
Fawbush, E. J., er al., Bull. Amer. Met. Soc. 32, 1-9, 1951.
Gallo, B. T., et al., Weather and Forecasting, 31(1), 273-295, 2016.
Hines, C. O., Can. J. Phys., 38, 1441–1481, 1960.
Mayr H.G., et al., Space Sci. Rev. 54, 297–375, 1990.
Miller, D. E., et al., Geophys. Res. Lett., 47, 2020.
Prikryl P., et al., Ann. Geophys. 27, 1-30, 2009a.
Prikryl P., et al., Ann. Geophys. 27, 31-57, 2009b.
Prikryl P., et al., J. Atmos. Sol.-Terr. Phys. 149, 219–231, 2016.
Prikryl P., et al., J. Atmos. Sol.-Terr. Phys. 171, 94–10, 2018.
Prikryl P., e al., J. Atmos. Sol.-Terr. Phys. 183, 36-60, 2019.
Prikryl P., et al., Ann. Geophys. 39 (4), 769–93, 2021a.
Prikryl P., et al., Atmosphere 12 (9), 2021b.
Prikryl P. & Rušin V., Front. Astron. Space Sci. 10, 2023.
Prikryl, P., Adv. Sci. Res., 21, 1–17, 2024.
Púčik, T., et al., Mon. Wea. Rev. 143, 4805–4821, 2015.
Púčik, T., et al., Technical memorandum, ECMWF, 2021. 10.21957/z0b3t5mrv
Tippett, M. K., Geophys. Res. Lett. 41, 6956–6961, 2014.
Wilcox, J. M., et al., Science 180 (4082): 185–86, 1973.

Supporting Information for poster EMS2024-392 | UP1.3

Occurrence of tornado outbreaks in the context of solar wind coupling to magnetosphere-ionosphere-atmosphere

Paul Prikryl[1], Vojto Rušin[2]

[1]Physics Department, University of New Brunswick, Fredericton, NB, Canada
[2]Astronomical Institute, Slovak Academy of Sciences, Tatranská Lomnica, Slovakia

Data and methods

The National Oceanic and Atmospheric Administration (NOAA) National Weather Service (NWS) storm database (https://www.ncdc.noaa.gov/stormevents/) contains records of significant weather episodes. The severe weather database is provided by the Storm Prediction Center http://www.spc.noaa.gov/wcm/#data, including a database of tornadoes. In Australia, the Bureau of Meteorology maintains the Severe Storm Archive including tornadoes (http://www.bom.gov.au/australia/stormarchive/).

The hourly reanalysis dataset ERA5 with spatial resolution of 0.25 x 0.25 degree (Hersbach et al., 2020) is a product of the European Centre for Medium-Range Weather Forecasts (ECMWF). Following Chen et al. (2018), indices including CAPE, slantwise CAPE (SCAPE), vertically integrated extent of realizable symmetric instability (VRS; a measure to quantify the "releasable" CSI) are diagnosed, to assess the likelihood of slantwise convection during tornado outbreaks.

The solar wind data are provided by the National Space Science Data Center (NSSDC) OMNIWeb http://omniweb.gsfc.nasa.gov (King and Papitashvili, 2005). The hourly averages of solar wind velocity, V, the interplanetary magnetic field (IMF) magnitude, $|\mathbf{B}|$, the standard deviation of IMF B_z, σ_{Bz}, and the proton density, n_p, are used to identify CIRs, the interfaces between the fast and slow solar wind at the leading edge of HSSs from coronal holes (Smith et al., 1976). The IMF sector boundaries (SBs) where the IMF reverses its polarity have been identified as heliospheric current sheets (HCSs) (Smith et al., 1978, Hoeksema et al., 1983) that usually closely precede, or sometimes coincide (Huang et al., 2016a, b), with stream interfaces. The high-density plasma (HDP) sheet ahead of HCS and stream interface leads to magnetic field compression that can cause recurring moderate to weak geomagnetic storms (Tsurutani et al., 1995). In the absence of the IMF data, magnetic sector boundary crossings, which are now generally referred to as HCS crossings, can be estimated from ground-based magnetograms (Svalgaard, 1975). In the present paper we use an updated list of SBs/HCSs (Prikryl et al., 2009a).

Measurements of the green coronal emission line intensity at 530.3 nm (Fe XIV) by ground-based coronagraphs from 1939 to 2008 have been merged into a homogeneous coronal dataset (Rybanský, 1975; Rybanský et al., 2001, 2005; Dorotovič et al., 2014; https://www.kozmos-online.sk). The coronal intensities are expressed in absolute coronal units (ACU) representing the intensity of the continuous spectrum from the center of the solar disk with a width of 1 Å at the same wavelength as the observational spectral line (1 ACU = 3.89 W $m^{-2}sr^{-1}$ at 530.3 nm). The intensity depletions, called coronal holes, are sources of HSSs. The green corona intensity for the solar central meridian is computed by averaging the intensities measured at the east and west limbs 14 days apart (Prikryl et al. 2009a).

The superposed epoch (SPE) method (e.g., Ambrož, 1979) is applied on time series of green corona intensity, solar wind parameters and tornado occurrence keyed to SB/HCS crossings, as well as other types of solar wind disturbances.

Occurrence of large tornado outbreaks

Tornado outbreaks are associated with different types of solar wind disturbances: large tornado outbreaks that closely followed CIRs (Type A); closely preceded HCSs/CIRs associated with HDP, including transient HCSs (Type B); closely followed impacts of ICMEs (Type C); and tornado outbreaks that occurred in the declining phase of major HSSs (Type D).

Figure S1 shows solar wind variables with the symbols on the time axis indicating HSS/CIRs arrivals, impacts of ICMEs, and the interplanetary magnetic field (IMF) sector boundary/HCS crossings. The IMF direction longitude is shown to identify magnetic sector boundaries as well as transient HCS crossings. Where available, the proxy magnetic field sectors (A: away, T: toward) are also indicated on the time axis. Large tornado outbreaks are highlighted in light green color. Outbreaks associated with recurrent HSSs are marked with asterisks.

In 1973 (Figure S1a), the arrivals of a recurrent HSS/CIR on May 6 and June 2, 1973 (one solar rotation apart) were closely followed by large tornado outbreaks (A*). Type B outbreaks were associated with HCS/HDP on May 28 and June 17, 1973. In 2009 (Figure S1b), the arrivals of a recurrent HSS/CIR on April 9 and May 6 were followed by large tornado outbreaks (A*). Type B outbreak on April 29/30 was associated with HCS/HDP at the end of April. Furthermore, a moderate outbreak occurred following the arrivals of HSS/CIRs on April 16, and two large outbreaks followed a minor and moderate HSS/CIRs on May 2 and 14, respectively.

Figure S1c shows tornado outbreak cases in May 2010 and January 2012. The arrivals of HSS/CIRs on May 10 and 19 were closely associated with large tornado outbreaks (A). Tornado outbreaks (B) on May 1-2 and 25-26 were associated with HCS/HDP on May 2 and 26, respectively. Two ICMEs on January 22 and 24, 2012, were followed by tornado outbreaks (C) on January 23 and 25, respectively.

In 2018 (Figure S1d), the arrivals of a recurrent HSS/CIR on October 7 and November 4 were followed by large tornado outbreaks as these HSSs started to decline (D*), while the next arrival of this recurrent HSS/CIR on December 1 was closely followed by a large outbreak (A*). A moderate outbreak on October 13 coincided with a strong HSS/CIR. Two large outbreaks (B) on October 2/3 and November 1 were associated with HCS/HDP.

SPE analysis of large tornado outbreaks relative to solar wind disturbances

Fig. S2 shows the SPE analysis of solar wind plasma variables and daily tornado occurrence keyed to CIRs, HCSs, IMCEs impacts and arrivals of HSS/CIRs associated with tornado outbreaks of Type A (35%), B (36%), C (11%) and D (18%), respectively. The peaks in cumulative numbers of tornadoes reflect the adopted classification of tornado outbreak occurrence that is predominantly of Type A and B (Figs. S2a and S2b). For Type A, B and D, the corresponding patterns of mean solar wind variables are similar to those shown in Fig. 1b in the poster. For Type B there is a broader density peak indicating superposition of HDP ahead of HCSs. For Type D the maximum mean velocity is highest indicating major HSSs. For Type C (Fig. S2c), as expected for interplanetary shocks ahead of ICMEs, the mean values of all four solar wind variables sharply increase at the key time.

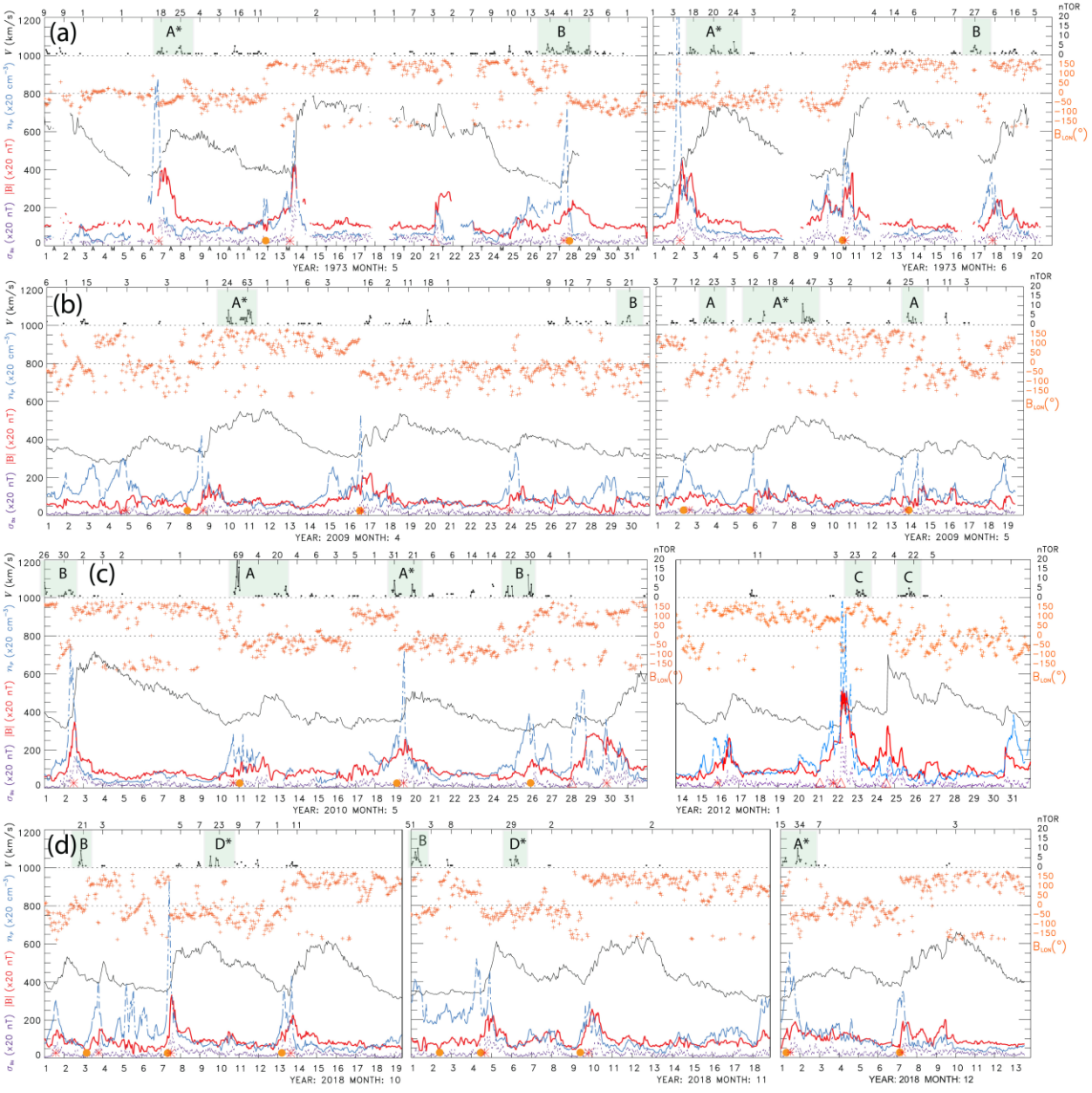

Figure S1: The OMNI solar wind V (solid black line), B (red), n_p (broken light blue line), σ_{Bz} (dotted purple line) with the y-axis scale factors shown on the left, and the magnetic field direction longitude (red crosses) with the y-axis shown on the right. The symbols at the time axis indicate (*) CIRs, (Δ) ICMEs, (●) HCS crossings, and where available, the proxy magnetic field sectors (A: away, T: toward). Hourly and daily numbers of tornadoes are shown at the top and days of tornado outbreaks are highlighted and labeled as Type A-D for periods in **(a)** May-June 1973, **(b)** April-May 2009, **(c)** May 2010, January 2012, and **(d)** October-December 2018. Outbreaks associated with recurrent HSSs are marked with asterisks.

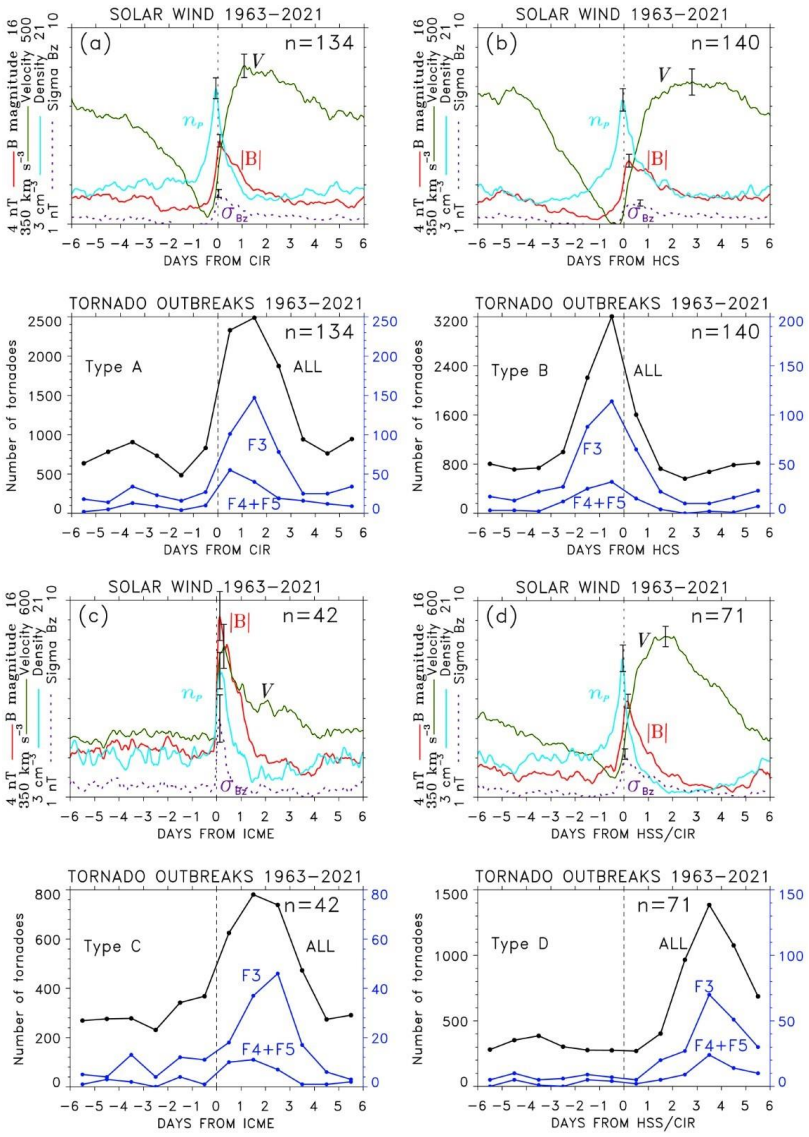

Figure S2. The SPE analysis of time series of solar wind plasma variables and tornado occurrence keyed to (**a**) CIRs, (**b**) HCSs, (**c**) ICMEs and (**d**) HSS/CIRs associated with large tornado outbreaks of Type A, B, C and D, respectively.

References

Ambrož, P. (1979). Statistical method of superposition of epochs. I-Methodical analysis and some criteria of application. *Bulletin of the Astronomical Institutes of Czechoslovak Academy of Sciences 30*, 114.

Chen, T.-C., Yau, M.K. & Kirshbaum, D.J. (2018). Assessment of conditional symmetric instability from global reanalysis data, *Journal of the Atmospheric Sciences, 75*, 2425–2443. https://doi.org/10.1175/JAS-D-17-0221.1.

Dorotovič, I., Minarovjech, M., Lorenc, M., and Rybanský, M. (2014). Modified homogeneous data set of coronal intensities, *Sol. Phys*., 289, 2697–2703, https://doi.org/10.1007/s11207- 014-0501-2, 2014.

Hersbach, H., Bell, B., and Berrisford, P, et al. (2020). The ERA5 global reanalysis. *Q J R Meteorol Soc.* 146, 1999– 2049. https://doi.org/10.1002/qj.3803

Hoeksema, J. T., Wilcox, J. M., & Scherrer, P. H. (1983). The structure of the heliospheric current sheet: 1978–1982. *Journal of Geophysical Research 88*, 9910–9918.

King, J. H., & Papitashvili, N. E. (2005). Solar wind spatial scales in and comparisons of hourly Wind and ACE plasma and magnetic field data. *Journal of Geophysical Research 110*, A02104. http://dx.doi.org/10.1029/2004JA010649

Prikryl, P. (2024). Mesoscale weather influenced by auroral gravity waves contributing to conditional symmetric instability release?. *Adv. Sci. Res., 21*, 1–17, https://doi.org/10.5194/asr-21-1-2024.

Prikryl, P., Rušin, V., Rybanský, M. (2009a). The influence of solar wind on extratropical cyclones – Part 1: Wilcox effect revisited. *Annales Geophysicae 27,* 1–30. doi:10.5194/angeo-27-1-2009

Prikryl, P., Muldrew, D. B., Sofko, G. J. (2009b). The influence of solar wind on extratropical cyclones – Part 2: A link mediated by auroral atmospheric gravity waves?. *Annales Geophysicae 27*, 31–57. doi:10.5194/angeo-27-31-2009

Richardson, I. G., Cliver, E. W., & Cane, H. V. (2000). Sources of geo- magnetic activity over the solar cycle: Relative importance of CMEs, high-speed streams, and slow solar wind, *Journal of Geophysical Research 105*, 18203–18213. https://doi.org/10.1029/1999JA000400

Richardson, I. G., Cliver, E. W., & Cane, H. V. (2001). Sources of geomagnetic storms for solar minimum and maximum conditions during 1972–2000, Geophysical Research Letters *28(13),* 2569-2572. https://doi.org/10.1029/2001GL013052

Richmond, A.D. (1978). Gravity wave generation, propagation, and dissipation in the thermosphere, *Journal of Geophysical Research 83*, 4131–4145.

Rotunno, R., & Klemp, J. B. (1982). The influence of the shear-induced pressure gradient on thunderstorm motion. *Monthly Weather Review 110,* 136–151.

Rotunno, R., & Klemp, J. B. (1985). On the rotation and propagation of simulated supercell thunderstorms. *Journal of Atmospheric Sciences 42*, 271–292.

Rybanský, M. (1975). Coronal index of solar activity, *Bulletin of the Astronomical Institutes of Czechoslovak Academy of Sciences 28*, 367–370.

Rybanský, M., Rušin, V., & Minarovijech, M. (2001). Coronal index of solar activity, *Space Science Reviews 95*, 227–234, 2001.

Rybanský, M., Rušin, V., Minarovjech, M., Klocok, L., & Cliver, E.W. (2005). Reexamination of the coronal index of solar activity, *Journal of Geophysical Research 110*, A08106, https://doi.org/10.1029/2005JA011146.

Smith, E. J.; Wolfe, J. H. (1976). Observations of interaction regions and corotating shocks between one and five AU: Pioneers 10 and 11. *Geophysical Research Letters 3*, 137–140, doi:10.1029/gl003i003p00137.

Smith, E. J., Tsurutani, B. T., & Rosenberg, R. L. (1978). Observations of the interplanetary sector structure up to heliographic latitudes of 16°: Pioneer 11, *Journal of Geophysical Research 83*, 717-724.

Svalgaard, L. (1975). On the use of Godhavn H component as an indicator of the interplanetary sector polarity, *Journal of Geophysical Research* 80, 2717-2722, https://doi.org/10.1029/JA080i019p02717

Tsurutani, B. T., Gonzalez, W. D., Gonzalez, A. L. C., Tang, F., Arballo, J. K., & Okada, M. (1995). Interplanetary origin of geomagnetic activity in the declining phase of the solar cycle. *Journal of Geophysical Research 100*, 21717–21733. http://dx.doi.org/10.1029/95JA01476

Wilcox, J. M., Scherrer, P. H., Svalgaard, L., Roberts, W. O., & Olson, R. H. (1973). Solar Magnetic Sector Structure: Relation to Circulation of the Earth's Atmosphere. *Science 180 (4082)*: 185–86. https://doi.org/10.1126/science.180.4082.185.

Wilcox, J. M., Scherrer, P. H., Svalgaard, L., Roberts, W. O., Olson, R. H., & Jenne, R. L. (1974). Influence of Solar Magnetic Sector Structure on Terrestrial Atmospheric Vorticity. *Journal of the Atmospheric Sciences 31(2)*: 581–88. https://doi.org/10.1175/1520-0469(1974)031<0581:IOSMSS>2.0.CO;2.